Trends and Descriptors of Heterogeneous Hydroformylation Activity and Selectivity of RhM3 (M = Fe, Co Ni, Cu and Zn) Catalysts

Journal:	*Catalysis Science & Technology*
Manuscript ID	CY-COM-05-2022-000821.R1
Article Type:	Communication
Date Submitted by the Author:	27-Jun-2022
Complete List of Authors:	Mao, Zhongtian; Brookhaven National Laboratory Department of Chemistry, Guo, Haoyue; Brookhaven National Laboratory, Chemistry Xie, Zhenhua; Brookhaven National Laboratory, Chemistry Division Liu, Ping; Brookhaven National Lab, Chemistry Chen, Jingguang; Columbia University, Chemical Engineering

COMMUNICATION

Trends and Descriptors of Heterogeneous Hydroformylation Activity and Selectivity of RhM_3 (M = Fe, Co Ni, Cu and Zn) Catalysts

Received 00th January 20xx,
Accepted 00th January 20xx

DOI: 10.1039/x0xx00000x

Zhongtian Mao,[a†] Haoyue Guo,[a†] Zhenhua Xie,[a,b,*] Ping Liu[a,*] and Jingguang G. Chen[a,b,*]

Monometallic Rh/MCM-41 and bimetallic RhM_3/MCM-41 (M = Fe, Co, Ni, Cu, Zn) catalysts are synthesized and tested for vapor-phase ethylene hydroformylation reaction. Co is found to exhibit a significant promotion effect on the selectivity of hydroformylation to C_3 oxygenate, followed by Fe and Cu, with Ni and Zn showing a negative effect. The DFT calculations reveal that the addition of the secondary metal can provide new type of sites, being able to selectively tune the binding energies of reaction intermediates and thus lead to different catalytic performances.

Supported Rh catalysts have drawn great attention as potential substitutes of homogeneous Rh catalysts for catalyzing light alkene hydroformylation.[1, 2] Comparing to homogeneous Rh catalysts, supported Rh catalysts exhibit numerous advantages such as easy catalyst separation, less precious metal loss, and robustness to air and moisture.[3, 4] However, the major challenge that hinders the application of supported Rh as heterogeneous catalysts is the difficulty to achieve comparable catalytic performance as their homogeneous counterparts. In most cases, monometallic Rh catalysts display low catalytic activity and low selectivity toward oxygenate products.[5, 6] The undesired hydrogenation reaction pathway is usually more favored than hydroformylation on monometallic Rh catalysts.[7, 8] A common strategy to enhance activity and selectivity is to add secondary components as promotors to form bimetallic systems, such as Co, Mo, Fe, V, Ag, Pd and alkali metals.[9, 10] Among these promotors, Co is one of the most widely used and has been studied extensively.[11, 12] In previous studies, it has been found that the addition of Co to supported Rh nanoparticles can increase the dispersion of Rh atoms and tune the binding energies of reaction intermediates via the close interaction between Rh and Co, resulting in improved overall catalytic activity and selectivity for hydroformylation.[13, 14] However, detailed mechanisms on the promotion effect of alloying the secondary metal with Rh still remain elusive, which can be of great importance leading to the rational optimization of Rh-based alloy catalysts for active and selective heterogeneous hydroformylation.

In this communication, systematic studies of catalytic behaviors going from monometallic Rh supported on MCM-41 (Rh/MCM-41) to Rh-based bimetallic catalysts with the addition of a secondary 3rd row transition metal M (RhM_3/MCM-41, M = Fe, Co, Ni, Cu, Zn) for the heterogeneous hydroformylation of ethylene were reported by combining experiments and density functional theory (DFT) calculations. The results of flow reactor studies at 200 °C among the six catalysts, $RhCo_3$/MCM-41 exhibits the highest yield and selectivity toward C_3 oxygenates, which is followed by $RhFe_3$ > $RhCu_3$, Rh_1 > $RhNi_3$ > $RhZn_3$ in a decreasing sequence of selectivity. Wherein, the selectivity of hydroformylation toward C_3 oxygenate has been measured at comparable ethylene conversion to ensure the comparability. According to the DFT calculations, the origin of the superior behavior of $RhCo_3$ is associated with the Rh-Co hybrid sites on the surface, being able to selectively weaken the CO binding and moderate the propanal binding via Co-induced strain and ensemble effects. In this way, the C-C coupling, the removal of propanal and thus the hydroformylation reaction can be facilitated. In contrast, the bimetallic effect is much less on the binding of hydrocarbon intermediates. The selective tuning of binding energies of the critical intermediates involved in ethylene hydroformylation is found to be essential in controlling the preference between ethylene hydroformylation to C_3 oxygenates and hydrogenation to ethane over the Rh-based bimetallic catalysts, and thus the activity/selectivity toward C_3 oxygenates.

The studies of catalytic activity were conducted in a flow reactor for 200 mg pure catalyst with a reaction stream of $C_2H_4/H_2/CO/N_2$ = 3/3/3/3 mL□min^{-1} at 200 °C. In **Fig. 1**, the conversion of C_2H_4 is plotted as a function of reaction time. The monometallic catalyst Rh_1 exhibits 22.3% C_2H_4 conversion, which is close to the results reported previously for the catalyst synthesized with similar methods.[14] For the bimetallic catalysts, the C_2H_4 conversion on $RhFe_3$ and $RhZn_3$ are lower than that on Rh_1, while $RhCu_3$, $RhCo_3$, and $RhNi_3$ show higher C_2H_4 conversion. All six catalysts reach a quasi-steady state C_2H_4

[a] Chemistry Division, Brookhaven National Laboratory, Upton, NY 11973.
[b] Department of Chemical Engineering, Columbia University, New York, NY 10027.
E-mail: zhenhuaxie@bnl.gov, pingliu3@bnl.gov, jgchen@columbia.edu
Electronic Supplementary Information (ESI) available: More details of experimental and theoretical method, DFT-calculated energies, and DFT-optimized structures. See DOI: 10.1039/x0xx00000x

†These authors contributed equally to this work.

conversion after 6 h. The data from 6 to 10 h are averaged and summarized in **Table 1**. $RhCo_3$ shows the best performance for catalyzing ethylene hydroformylation. The total C_3 oxygenates (propanal and 1-propanol) yield on $RhCo_3$ is 8.5%, which is the highest among the six catalysts. In our previous work, a $RhCo_3$ catalyst with better metal dispersion and higher CO uptake showed higher oxygenate selectivity[14] than the current study. This is consistent with the literature that a better Rh dispersion reduces the hydrogenation activity and thus enhances hydroformylation selectivity[15-17]. $RhNi_3$ shows the highest C_2H_4 conversion of 75.0%. However, the undesired ethane yield on $RhNi_3$ is also the highest, and the yield to C_3 oxygenates is only 3.5%. The C_2H_4 conversion on $RhFe_3$ and $RhZn_3$ are much lower than other bimetallic catalysts, mostly due to insufficient active metal sites as suggested by the CO uptake values.

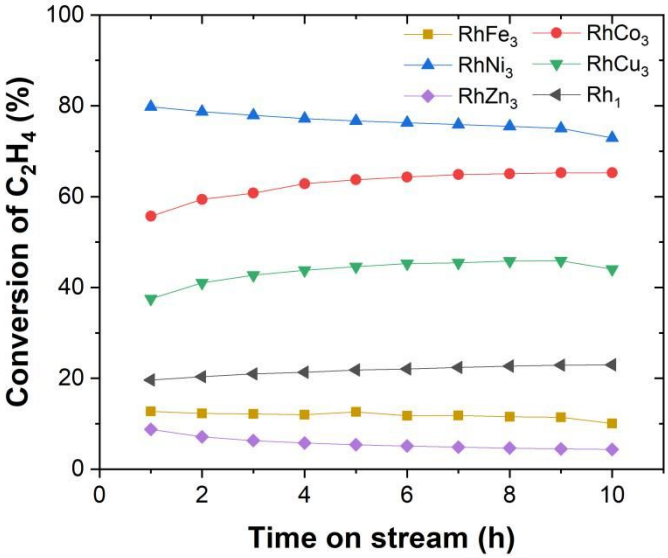

Fig. 1 Conversion of C_2H_4 on Rh/MCM-41 and RhM_3/MCM-41 catalysts. Reaction conditions: 200 °C, $C_2H_4/H_2/CO/N_2$ = 3/3/3/3 mL·min^{-1}, catalyst mass = 200 mg, 60-80 mesh, atmospheric pressure.

Table 1 Catalytic performance of Rh/MCM-41 and RhM_3/MCM-41 catalysts. Reaction conditions: 200 °C, $C_2H_4/H_2/CO/N_2$ = 3/3/3/3 mL·min^{-1}, catalyst mass = 200 mg, 60-80 mesh, atmospheric pressure.

Catalysts	CO Uptake (μmol·g^{-1})	C_2H_4 Conversion (%)	TOF (min^{-1})			C_2H_4-based Yield (%)		
			C_2H_4	C_3H_6O	C_3H_8O	C_2H_6	C_3H_6O	C_3H_8O
Rh_1	54.7	22.3	2.2	0.3	0.0	19.8	2.5	0.0
$RhFe_3$	17.5	12.0	2.4	0.5	0.3	9.0	1.7	1.1
$RhCo_3$	77.8	64.5	4.2	0.3	0.3	55.7	4.4	4.1
$RhNi_3$	114.2	75.0	3.5	0.1	0.0	70.9	2.8	0.7
$RhCu_3$	48.3	45.5	4.7	0.5	0.1	40.3	4.3	0.9
$RhZn_3$	21.5	4.9	1.2	0.2	0.0	4.2	0.6	0.1

The studies performed for 200 mg pure catalyst do not show the trend in selectivity due to the significant variation in C_2H_4 conversion (4.9-75.0%). To compare the selectivity under comparable C_2H_4 conversions, Rh_1, $RhCo_3$, $RhNi_3$, and $RhCu_3$ are diluted with the support material MCM-41. The dilution ratios (i.e., mass ratio of pure catalyst to the MCM-41 support) are given in **Table 2**. Due to the low activity of $RhZn_3$, the catalyst mass of $RhZn_3$ is increased from 200 mg to 400 mg to achieve comparable C_2H_4 conversion to other catalysts. The selectivity toward ethane and C_3 oxygenates for the six catalysts are compared in **Table 2**. The C_3 oxygenates selectivity follows the trend of $RhCo_3$ > $RhFe_3$ > $RhCu_3$, Rh_1 > $RhNi_3$ > $RhZn_3$, with $RhCo_3$ exhibiting the highest selectivity of 30.8% toward C_3 oxygenates. Even though the $RhCo_3$ catalyst showed lower activity and oxygenate selectivity than those reported in 1990s,[18-22] here we focus on exploring the trend and descriptors of heterogeneous hydroformylation activity and selectivity over the RhM_3 catalysts. It is noted that most of the early reported heterogeneous RhCo catalysts (e.g., $RhCo_3/SiO_2$) were synthesized with metal carbonyl complexes, such as $Rh_4(CO)_{12}$, $Co_2(CO)_8$, and/or $RhCo_3(CO)_{12}$ clusters. They generally exhibited a higher metal dispersion and higher alloying extent (i.e., stronger Rh-Co interaction) than the metal nitrate-derived catalysts in the present work. The focus of the current work is to identify trends and descriptors of heterogeneous hydroformylation activity and selectivity over the RhM_3 catalysts synthesized by the same method.

Table 2. Catalytic performance of Rh/MCM-41 and RhM_3/MCM-41 catalysts under comparable C_2H_4 conversion. Reaction conditions: 200 °C, $C_2H_4/H_2/CO/N_2$ = 3/3/3/3 mL·min^{-1}, 60-80 mesh, atmospheric pressure.

Catalyst	Dilution Ratio[a]	Total Catalyst loading (mg)	C_2H_4 Conversion (%)	C_2H_4-based Selectivity (%)		
				C_2H_6	C_3H_6O	C_3H_8O
Rh_1	1:3	200	10.4	83.8	15.9	0.1
$RhFe_3$	1:0	200	12.0	75.1	14.0	9.3
$RhCo_3$	1:15	200	7.9	68.8	28.0	2.8
$RhNi_3$	1:9	200	12.0	87.3	12.7	0.0
$RhCu_3$	1:9	280	8.4	83.7	15.8	0.5
$RhZn_3$	1:0	400	7.9	89.1	9.9	1.0

[a]: The dilution ratio was defined as the mass ratio of pure catalyst to the MCM-41 support. Note: The remaining selectivity for Rh_1 (0.2%), $RhFe_3$ (1.6%), and $RhCo_3$ (0.4%) was associated with the formation of a minor amount of C_3H_6 and C_3H_8.

The DFT calculations were performed to gain an atomic level understanding for ethylene hydroformylation on the supported Rh_1 and RhM_3 (M = Co, Ni, Cu). To determine the surface configurations of a RhM_3 bimetallic catalyst, three types of (111) slab models were considered following the approach used previously.[23] The bulk-terminated RhM_3(111) surface was used to describe the stoichiometric conformation, and the skin Rh/M(111) and the sandwich M/Rh/M(111) structures were also explored to simulate the two extreme cases of surface segregation. The results show that thermodynamically the three alloys considered favor the bulk-terminated surfaces(**Table S1**), consistent with the previous study of $RhCo_3$[14]. Accordingly, the bulk-terminated surfaces were used to describe the catalytic behaviors of RhM_3 on exposure to CO, hydrogen, and C_2H_4, where single Rh atom was isolated by M on the surface (**Fig. 2**). As demonstrated below, such conformation introduces both strain and ensemble effects, which enable the tuning of binding properties and thus the catalytic selectivity for ethylene hydroformylation. The $RhFe_3$ and $RhZn_3$ catalysts were not included, which showed lower conversion of C_2H_4 than Rh_1

according to the reactor results (**Fig. 1**). On the other hand, the situation for $RhFe_3$ and $RhZn_3$ is rather complex. Fe or Zn prefers to be partially oxidized and it is difficult to determine the exact structures of FeO_x/Rh or ZnO/Rh in theory, which can affect the selectivity significantly.

The reaction starts with the adsorption of CO and C_2H_4, where CO prefers the Rh_3 hollow site on Rh(111) (*CO) and the

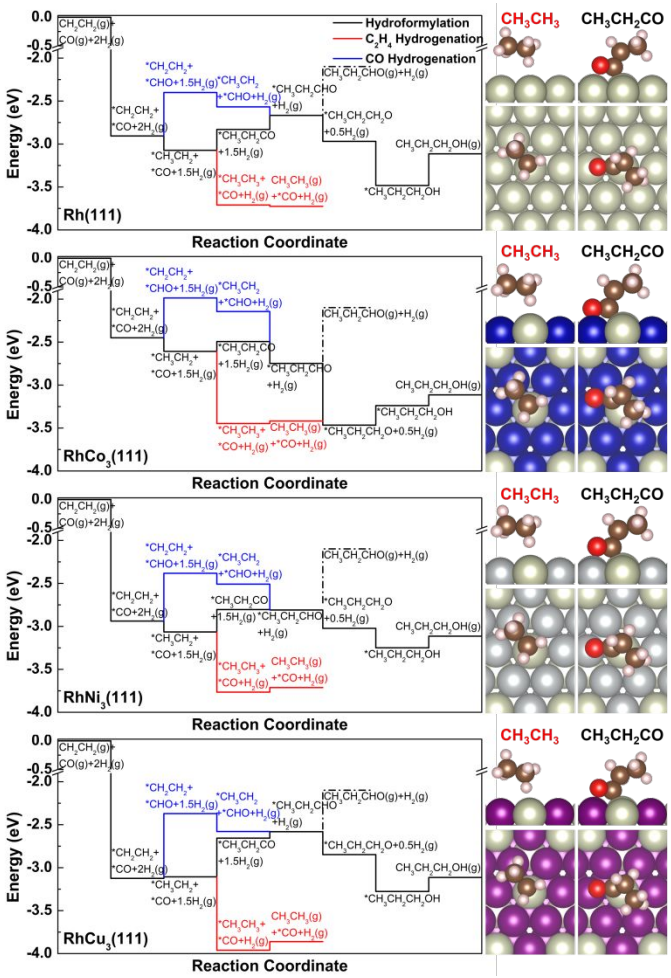

Fig. 2 Left panel: Potential energy diagrams of hydroformylation of ethylene *vs* hydrogenation of ethylene *vs* hydrogenation of CO over Rh(111), $RhCo_3$(111), $RhNi_3$(111) and $RhCu_3$(111) surfaces. Right panel: Corresponding optimized structures for $*CH_3CH_3$ and $*CH_3CH_2CO$ (H: white; C: brown; O: red; Rh: cream; Co: blue; Ni: silver; Cu: purple).

hybrid RhM_2 hollow sites due to the ensemble effect on $RhCo_3$(111), $RhNi_3$(111) and $RhCu_3$(111) (**Fig. 2**). While the Rh top site is favored for the adsorption of C_2H_4 ($*CH_2CH_2$) and C_3H_6 ($*CH_3CH_3$) on the surfaces studied (**Fig. S1-S5**). Compared to Rh, the bindings of both reactants are weakened by alloying with Co, where more significant effect for CO (BE = -1.65 eV) than C_2H_4 is observed (**Fig. S1**). This is associated with the strain effect introduced by Co on the surface, which results in a shortened bond between surface Rh with the nearest neighbors (2.52 Å for $RhCo_3$ vs. 2.70 Å for Rh) and therefore more significant downshift of Rh d-band than that of Ni and Cu (**Fig. S6**). In addition, the ensemble effect leads to the formation of the Co_3 ensemble on the surface with a shorter Co-Co bond (2.48 Å) than the bulk Co (2.51 Å) and a lower-lying Co d-band (**Fig. S6**). Given that, the weakened *CO binding is expected according to the d-band theory[24]. The only exception is $RhCu_3$(111), where the Rh top site is preferred due to the Cu d-band being away from the Fermi level (**Fig. S6**); while Rh corresponds to a high-lying d-band and binds CO the most strongly (BE= -2.09 eV) among the systems studied.

The subsequent hydrogenation of adsorbed $*CH_2CH_2$ and *CO produces $*CH_3CH_2$ and *CHO, respectively. Over the four surfaces the formation of $*CH_3CH_2$ is slightly exothermic, but more thermodynamically favorable than the competing formation of *CHO. Along the hydroformylation pathway, the C-C coupling can proceed via *CO and $*CH_3CH_2$ to form $*CH_3CH_2CO$ or via *CHO and $*CH_3CH_2$ to form $*CH_3CH_2CHO$, where in both cases the adsorbate is adsorbed at the Rh-M hybrid site via maintaining the Rh-C bond and forming the new M-O bond (**Fig. S2-S5**). As shown in **Fig. 2**, the -CO insertion is slightly uphill on the surfaces studied with the lowest reaction energy observed for $RhCo_3$(111) (ΔE= 0.11 eV) due to the significantly weakened surface-CO interaction and thus facilitated C-C bond coupling. Indeed, the strong surface-CO interaction was found previously to hinder the ethanol synthesis via -CO insertion mechanism during CO hydrogenation on Rh(111)[25]. The hydrogenation of $*CH_3CH_2CO$ to $*CH_3CH_2CHO$ is also slightly more favorable on $RhCo_3$(111) (ΔE= -0.25 eV) than the other surfaces (ΔE: 0.00~0.18 eV) (**Fig. 2**). The desorption of $*CH_3CH_2CHO$ is endothermic on the selected surfaces (ΔE: 0.48-0.71eV**, Fig. 2**), which can hinder the production of CH_3CH_2CHO; by comparison, the further hydrogenation to $*CH_3CH_2CH_2O$ is more thermodynamically preferred and again $RhCo_3$(111) shows the most exothermicity (ΔE= -0.72 eV). The formation of $*CH_3CH_2CH_2OH$ via the further hydrogenation of $*CH_3CH_2CH_2O$ is uphill in energy of 0.23 eV on $RhCo_3$(111) and releases energies on other surfaces (ΔE< -0.2 eV). Finally, the desorption of $*CH_3CH_2CH_2OH$ is slightly endothermic (ΔE: 0.10~0.37 eV eV), which is likely feasible under the experimental conditions of hydroformylation.

Alternatively, along the C_2H_4 hydrogenation pathway $*CH_3CH_2$ is further hydrogenated to produce $*CH_3CH_3$. The DFT results show that it is energetically more favorable than the C-C coupling (ΔE < -0.5 eV) along the hydroformylation pathway and the subsequent $*CH_3CH_3$ desorption is also facile (ΔE< 0.05 eV) over the four selected surfaces. Compared to the hydroformylation pathway, the tuning of bindings to the intermediates along hydrogenation pathway due to alloying is less significant (**Fig. S1**).

According to the DFT calculated energetics, upon exposure to CO, C_2H_4 and H_2, thermodynamically hydroformylation prefers to proceed via $*CH_2CH_2$ + *CO →$*CH_3CH_2$ + *CO→ $*CH_3CH_2CO$→$*CH_3CH_2CHO$→$*CH_3CH_2CH_2O$ → $*CH_3CH_2CH_2OH$ over Rh(111), $RhCo_3$(111), $RhNi_3$(111) and $RhCu_3$(111) surfaces (**Fig. 2**). The hydroformylation via the -CHO insertion to $*CH_3CH_2$ is less competitive, which has been previously proposed to facilitate the C–C coupling on the Cs-decorated Cu/ZnO catalysts[26]. This is associated with the much stronger binding to CO than C_2H_4, which leads to the preferential hydrogenation of $*CH_2CH_2$ to $*CH_2CH_3$ over that of *CO to *HCO on the Rh and

RhM_3 surfaces (**Fig. 2**). In addition, different from the previous study[26], *CHO is not stable enough to initiate the C-C coupling on Rh-based surfaces, but favoring the decomposition back to *CO.

The experimentally observed trend in selectivity can be well described based on the DFT-calculated differences in energy. The higher CH_3CH_3 selectivity over C_3 oxygenates (CH_3CH_2CHO and $CH_3CH_2CH_2OH$) for the studied systems (**Table 2**) can be demonstrated by the thermodynamic preference of $*CH_3CH_2$ hydrogenation to CH_3CH_3 over the C-C coupling with *CO (**Fig. 2**). In addition, the desorption of $*CH_3CH_2CHO$ and thus the production of CH_3CH_2CHO is less favorable than hydrogenation to $*CH_3CH_2CH_2O$ according to the reaction energy (**Fig. 2**). However, higher CH_3CH_2CHO selectivity over $CH_3CH_2CH_2OH$ for the Rh-based systems is observed experimentally (**Table 2**). Given that, the energy cost for desorption can be compensated by the entropic contribution at the reaction temperature of 200 °C. Consequently, the majority of $*CH_3CH_2CHO$ desorbs, and only small fraction undergoes the competing hydrogenation to $CH_3CH_2CH_2OH$.

As indicated above, the high selectivity of C_3 oxygenates depends on the facile C-C coupling between $*CH_3CH_2$ and *CO

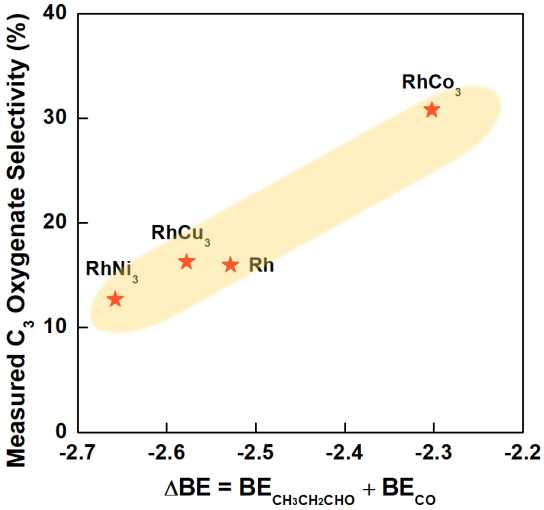

Fig. 3 Correlation of DFT-calculated sum of binding energies of $*CH_3CH_2CHO$ and *CO with the experimentally measured C_3 oxygenate selectivity on Rh, $RhCo_3$ $RhCu_3$ and $RhNi_3$ at the comparable conversion.

as well as the fast removal of $*CH_3CH_2CHO$. One can see that the bond-tuning on the hydrocarbon intermediates introduced by alloying is much less significant than that on the oxygenate intermediates involved (**Fig. S1**). Thus, the binding to the oxygenates can be critical in controlling the selectivity. Specifically, a positive shift in the binding energies of *CO and/or $*CH_3CH_2CHO$ can help increase the selectivity to C_3 oxygenates on the Rh-based catalysts. Indeed, the experimentally measured decreasing sequence in selectivity of C_3 oxygenates, $RhCo_3$ > Rh, $RhCu_3$ > $RhNi_3$, can be well captured by the negative shift in the sum of binding energies of *CO and $*CH_3CH_2CHO$ on each surface (**Fig. 3**). In general, the weaker the binding of *CO and/or $*CH_3CH_2CHO$ is, the higher the selectivity to C_3 oxygenate becomes. Here, since the *CO binding is stronger than $*CH_3CH_2CHO$ (**Fig. S1**) and the -CO insertion is more energetically challenging than the removal of $*CH_3CH_2CHO$ (**Fig. 2**), the weakening of *CO binding is likely to dominantly control the selectivity and the effect from $*CH_3CH_2CHO$ binding can be secondary. Following such principle, with the weakest CO binding (BE= -1.65 eV) and moderate $*CH_3CH_2CHO$ interaction (BE= -0.65 eV), $RhCo_3$ displays the highest C_3 oxygenate electivity among the systems studied (**Fig. S1 and 3**). In the case of $RhCu_3$, although the *CO binding is the strongest (BE= -2.09 eV), the weakest binding to $*CH_3CH_2CHO$ (BE= -0.48 eV) help compensate and enable the C_3 selectivity comparable to Rh as observed experimentally (**Fig. S1 and 3**). For $RhNi_3$, the *CO binding is as strong as that of Rh (BE= -1.95 eV); yet it interacts with $*CH_3CH_2CHO$ most strongly (BE= -0.71 eV), leading to a lower selectivity than Rh. Here, we note that the trend between DFT-calculated sum of binding energies of $*CH_3CH_2CHO$ and *CO and the experimentally measured C_3 oxygenate selectivity can be meaningful only within a certain range: -2.7 eV < sum of binding energy < -2.3 eV. It is possible that further positive shifts of the sum of binding energy, or weakening in the $*CO/*CH_3CH_2CHO$ binding, may be associated with the destabilization of other reaction intermediates and thus decrease the C_3 oxygenate selectivity. More systematic studies of additional catalysts are required to determine whether the binding energy range can be extended in Figure 3.

In conclusion, the $RhCo_3$/MCM-41 bimetallic catalyst was found to exhibit higher catalytic performance in both the yield and the selectivity of C_3 oxygenates than Rh/MCM-41 and RhM_3/MCM-41 (M=Fe, Ni, Cu, Zn) for ethylene hydroformylation using a flow reactor at 200 °C. The experimentally observed sequence in C_3 selectivity, $RhCo_3$ > Rh, $RhCu_3$ > $RhNi_3$ was well captured by the DFT-calculated binding energies of *CO and $*CH_3CH_2CHO$. The superior C_3 selectivity of $RhCo_3$ is associated with the effectively weakened *CO interaction and thus the facilitated C-C coupling with $*CH_3CH_2$, while the $*CH_3CH_2CHO$ binding is moderate to allow its facile removal to complete the catalytic cycle. Wherein, the interplay between the ensemble effect, which limits the strong adsorption on the high symmetric Rh_3 hollow site, and the compressive strain effect, which down-shifts the d-band of surface Co and Rh atoms plays an essential role.

This work was supported by the US Department of Energy, Office of Basic Energy Sciences, Division of Chemical Sciences, Geosciences, & Biosciences, and carried out at Brookhaven National Laboratory, operated under contract DE-SC0012704. The DFT calculations were performed using computational resources at the Center for Functional Nanomaterials, a user facility at Brookhaven National Laboratory, and at the National Energy Research Scientific Computing Center, which is supported by the Office of Science of the U.S. DOE under Contract No. DE-AC02-05CH11231.

Conflicts of interest

There are no conflicts to declare.

Notes and references

1. J. Amsler, B. B. Sarma, G. Agostini, G. Prieto, P. N. Plessow and F. Studt, *J. Am. Chem. Soc.*, 2020, **142**, 5087-5096.
2. S. Lee, A. Patra, P. Christopher, D. G. Vlachos and S. Caratzoulas, *ACS Catal.*, 2021, **11**, 9506-9518.
3. M. Tan, D. Wang, P. Ai, G. Liu, M. Wu, J. Zheng, G. Yang, Y. Yoneyama and N. Tsubaki, *Appl. Catal., A*, 2016, **527**, 53-59.
4. J. Amsler, B. B. Sarma, G. Agostini, P. N. Plessow and F. Studt, *J. Am. Chem. Soc*, 2020, **142**, 5087-5096.
5. N. Huang, B. Liu, X. Lan and T. Wang, *Ind. & Eng. Chem. Res.*, 2020, **59**, 18771-18780.
6. S. Hanf, L. A. Rupflin, R. Gläser and S. A. Schunk, *Catalysts*, 2020, **10**, 510.
7. M. Lenarda, L. Storaro and R. Ganzerla, *J. Mol. Catal.*, 1996, **111**, 203-237.
8. M. Lenarda and R. Ganzerla, *J. Mol. Catal.*, 1992, **72**, 75-84.
9. L. Sordelli, M. Guidotti, D. Andreatta, G. Vlaic and R. Psaro, *J. Mol. Catal.*, 2003, **204-205**, 509-518.
10. B. Liu, N. Huang, Y. Wang, X. Lan and T. Wang, *ACS Catal.*, 2021, **11**, 15235-15243.
11. N. Huang, B. Liu, X. Lan and T. Wang, *Ind. Eng. Chem. Res.*, 2020, **59**, 18771-18780.
12. L. Zhang, C. Li, Y. Ma and T. Wang, *Prog. React. Kinet. Mech.*, 2018, **43**, 136-143.
13. Z. Mao, Z. Xie and J. G. Chen, *ACS Catal.*, 2021, **11**, 14575-14585.
14. Z. Xie, Y. Xu, M. Xie, X. Chen, J. H. Lee, E. Stavitski, S. Kattel and J. G. Chen, *Nature Commun.*, 2020, **11**, 1887.
15. S. M. McClure, M. Lundwall and D. Goodman, *Proc. Natl. Acad. Sci. U.S.A.*, 2011, **108**, 931-936.
16. T. Hanaoka, H. Arakawa, T. Matsuzaki, Y. Sugi, K. Kanno and Y. Abe, *Catal. Today*, 2000, **58**, 271-280.
17. S. Hanf, L. Alvarado Rupflin, R. Gläser and S. A. Schunk, *Catalysts*, 2020, **10**, 510.
18. L. Huang, Y. Xu, G. Piao, A. Liu and W. Zhang, *Catal. Lett.*, 1994, **23**, 87-95.
19. L. Huang, *J. Mol. Catal. A: Chem.*, 1997, **125**, 47-52.
20. L. Huang and Y. Xu, *Catal. Lett.*, 1996, **40**, 203-206.
21. L. Huang, A. Liu and Y. Xu, *Journal of Molecular Catalysis A: Chemical*, 1997, **124**, 57-66.
22. F. Ungváry, *Coord. Chem. Rev.*, 1998, **170**, 245-281.
23. Z. Xie, X. Wang, X. Chen, P. Liu and J. G. Chen, *J. Am. Chem. Soc.*, 2022, **144**, 4186-4195.
24. B. Hammer, J. Norskov, B. Gates and H. Knozinger, *Adv. Catal.*, 2000, **45**, 71-129.
25. Y. Choi and P. Liu, *J. Am. Chem. Soc.*, 2009, **131**, 13054-13061.
26. X. Wang, P. J. Ramírez, W. Liao, J. A. Rodriguez and P. Liu, *J. Am. Chem. Soc.*, 2021, **143**, 13103-13112.